https://doi.org/10.5194/egusphere-2026-4942
Preprint. Discussion started: 19 August 2026

Strong Cloud-Mediated Aerosol Cooling in TaiESM1 Diagnosed Using Cloud Radiative Kernels and APRP Decomposition

I-Chun Tsai, Chein-Jung Shiu, Cheng-An Chen, Hsin-Chien Liang, Hung-Hsiung Hsu, and Wei-Liang Lee

Research Center for Environmental Changes, Academia Sinica, Taipei, Taiwan, R. O. C.

*Corresponding author:
Chein-Jung Shiu
Research Center for Environmental Changes
Academia Sinica
128 Academia Road, Section 2, Nankang,
Taipei, Taiwan 11529, R. O. C.
Email: cjshiu @gate.sinica.edu.tw

https://doi.org/10.5194/egusphere-2026-4942
Preprint. Discussion started: 19 August 2026

Abstract

Aerosol–cloud interactions remain a major uncertainty in estimating human influence on climate. Here, we diagnose how aerosols, clouds, radiation, and ocean coupling interact in the Taiwan Earth System Model version 1 (TaiESM1). We use two complementary diagnostic methods to separate cloud radiative responses, aerosol-mediated effects, and the roles of aerosol–cloud and aerosol–radiation interactions. The contrast between the historical simulation and the pre-industrial control simulation produces a strongly negative total cloud radiative response (−2.08 W m^{-2}), dominated by an aerosol-mediated component (−2.24 W m^{-2}), despite a positive global-mean cloud feedback (+0.84 W m^{-2} K^{-1}). This cooling is concentrated over the North Pacific and North Atlantic, where changes in low- and middle-level clouds are associated with stronger reflection of solar radiation. The shortwave aerosol effective radiative forcing is −2.34 W m^{-2}, mainly from aerosol–cloud interactions (−2.00 W m^{-2}), while aerosol–radiation interactions are weaker (−0.34 W m^{-2}). Within the aerosol–cloud component, cloud scattering dominates (−2.14 W m^{-2}), whereas cloud-amount changes are small and positive (+0.12 W m^{-2}). Compared with selected Coupled Model Intercomparison Project Phase 6 models, TaiESM1 lies near the strong aerosol–cloud cooling end of the sample. Fully coupled and prescribed-sea-surface-temperature simulations indicate that ocean coupling mainly alters regional patterns rather than the global-mean magnitude. These results identify cloud scattering of sunlight as the dominant driver of TaiESM1's aerosol-related cloud cooling and highlight aerosol activation, cloud droplet number, and cloud optical depth as priorities for model development.

Keywords: Aerosol, Cloud, Aerosol-Cloud Interactions, Taiwan Earth System Model, CMIP6

https://doi.org/10.5194/egusphere-2026-4942
Preprint. Discussion started: 19 August 2026

1 Introduction

Clouds remain a leading source of uncertainty in climate projections because they respond simultaneously to greenhouse-gas-induced warming and anthropogenic aerosol perturbations. This uncertainty is closely tied to the spread in equilibrium climate sensitivity, as recent CMIP6 analyses have shown that higher-sensitivity models tend to exhibit stronger positive cloud feedbacks, particularly through changes in low-cloud amount and albedo (Zelinka et al., 2020). Broader assessments of climate sensitivity also identify cloud feedback, especially from marine low clouds, as a central process that limits the constraint on future warming (Sherwood et al., 2020). In parallel, anthropogenic aerosols exert a substantial but uncertain cooling influence through aerosol–radiation interactions and aerosol–cloud interactions, with the latter remaining particularly difficult to constrain because it depends on aerosol activation, cloud microphysical adjustment, liquid water path, cloud amount, and cloud radiative properties (Bellouin et al., 2020; Smith et al., 2020). Although greenhouse-gas-driven cloud feedback and aerosol–cloud interactions are physically distinct, they are radiatively coupled in historical climate simulations. C. Wang et al. (2021) indicated that CMIP6 models with stronger positive cloud feedback tend to produce stronger negative aerosol-mediated cloud radiative responses, leading to a compensation between greenhouse-gas-driven cloud feedback and aerosol-induced cooling over the historical period. This compensation complicates the interpretation of historical warming trends because models with markedly different combinations of cloud feedback and aerosol–cloud interaction strength can nonetheless reproduce comparable global-mean temperature trajectories.

Aerosol–cloud interactions remain difficult to constrain because they involve a sequence of coupled microphysical and macrophysical processes. Increased aerosol loading can enhance cloud droplet number concentration and reduce droplet effective radius, thereby increasing cloud albedo through the Twomey effect (Twomey, 1974; Twomey, 1977). Smaller and more numerous droplets can also suppress collision–coalescence and precipitation formation, potentially modifying cloud lifetime, liquid water path, and cloud fraction (Albrecht, 1989). However, these adjustments are not necessarily monotonic, because cloud responses depend on boundary-layer humidity, stability, precipitation regime, entrainment, and cloud type. Large-eddy simulations have shown that absorbing aerosols and aerosol-induced thermodynamic adjustments can either enhance or suppress cloud cover depending on the vertical distribution of heating and cloud-regime conditions (Ackerman et al., 2000). These process dependencies explain why aerosol–cloud interactions cannot be inferred from aerosol optical depth alone and why model-specific diagnostics of aerosol activation, cloud optical properties, and cloud-radiative effects are required. Recent satellite-based constraints further show that liquid-water-path and cloud-fraction adjustments can contribute substantially to aerosol–cloud interactions over marine liquid clouds, while the cloud-droplet activation response to aerosol perturbations may be weaker than a one-to-one relationship would imply (Park et al., 2025; Wall et al., 2023). These findings underscore the need to evaluate the full aerosol–activation–cloud optical pathway rather than relying solely on aerosol optical depth.

The Taiwan Earth System Model version 1 (TaiESM1) offers an instructive case for such a diagnosis. The model has previously been applied to investigate aerosol impacts on the East Asian winter monsoon and associated regional climate responses, demonstrating the ability of TaiESM1 to capture key aerosol–circulation linkages over East Asia (Tsai et al., 2024). Its cloud representation has also been evaluated for diurnal-cycle biases, revealing that cloud timing and cloud-regime-dependent processes remain important targets for continued model evaluation and development (Tsai et al., 2025). Nevertheless, a systematic diagnosis of TaiESM1's aerosol-mediated cloud radiative response, its relation to cloud feedback, and its decomposition into aerosol–radiation and aerosol–cloud components has not yet been undertaken.

This study therefore examines how aerosol perturbations shape the cloud radiative response in TaiESM1 and whether the resulting cooling is primarily mediated through cloud processes. We first quantify the aerosol-mediated cloud radiative response relative to the model's cloud feedback using the cloud radiative kernel framework of C. Wang et al. (2021). We then apply the APRP-based effective radiative forcing (ERF) decomposition of Zelinka et al. (2023) to determine whether the historical aerosol-related shortwave cooling is driven primarily by aerosol–radiation interactions or aerosol–cloud interactions. This combined approach links the historical aerosol-mediated cloud radiative response with its shortwave radiative components, allowing us to determine whether TaiESM1's aerosol-related cooling is controlled mainly by aerosol–radiation or aerosol–cloud interactions. The remainder of the paper describes the model experiments and diagnostic methods in Sect. 2, presents the cloud radiative response and APRP decomposition in Sect. 3, and discusses the implications for TaiESM1 aerosol–cloud coupling and future model development in Sect. 4.

2 Model experiments and diagnostic methods

This section describes the TaiESM1 simulations and diagnostic methods used in this study. We first introduce the model configuration and experimental design. We then describe two complementary diagnostics: a cloud radiative kernel method for separating cloud feedback from aerosol-mediated cloud radiative response, and an APRP-based decomposition for partitioning shortwave aerosol forcing into aerosol–radiation and aerosol–cloud components. These methods together provide a consistent framework for linking TaiESM1's historical cloud radiative response to aerosol-induced changes in cloud and radiative properties.

2.1 TaiESM1 Description and Simulation Configuration

TaiESM1 was developed from the National Center for Atmospheric Research Community Earth System Model version 1.2.2 (CESM1.2.2; (Hurrell et al., 2013)), with updated physical parameterizations including the GTS cloud-fraction scheme (Shiu et al., 2021), the Statistical-

https://doi.org/10.5194/egusphere-2026-4942
Preprint. Discussion started: 19 August 2026

Numerical Aerosol Parameterization (SNAP; (Chen et al., 2013)), three-dimensional radiation–topography interactions (Lee et al., 2019), and improved trigger functions for deep convection (Wang et al., 2015). The model realistically reproduces the mean climate state and several key climate features, including diurnal rainfall variability, monsoon evolution, and large-scale teleconnections (Lee et al., 2020; Y.-C. Wang et al., 2021). The atmospheric component has a horizontal resolution of approximately 1° × 1° with 30 vertical levels, and aerosol microphysical processes, cloud microphysics, and radiative transfer are interactively coupled. In TaiESM1, aerosols act as both cloud-condensation and ice-nucleation particles, enabling fully interactive aerosol–cloud processes, including droplet activation, rainout, and washout. This coupling allows the present framework to distinguish radiative effects arising from temperature-driven cloud feedback from those induced by aerosol perturbations, thereby supporting a comprehensive assessment of aerosol–cloud interactions in the model.

Building on previous evaluations of TaiESM1's aerosol and cloud representations, this study examines the model's response to distinct aerosol-related forcing pathways using CMIP6-protocol experiments and complementary sensitivity simulations (Collins et al., 2017; Eyring et al., 2016). Specifically, we analyze the fully coupled historical simulation, the pre-industrial control run, the near-term-climate-forcer perturbation experiment piNTCF, a TaiESM1 aerosol-only sensitivity simulation driven by historical aerosol emissions, and a prescribed-SST historical experiment, histSST. The experimental design is summarized in Table 1, which lists the forcing configuration, SST or ocean treatment, and primary diagnostic role of each experiment. Together, these simulations allow us to separate the fully coupled historical response, the prescribed-SST historical response, the aerosol-forced response under a pre-industrial background state, and the interactive-ocean residual. All diagnostics are based on monthly mean model output for 1985–2014, using the same period across experiments to evaluate cloud and radiative responses.

2.2 Cloud Radiative Kernel Diagnosis

To isolate the contribution of clouds to the total radiative response, we apply the radiative kernel method of C. Wang et al. (2021), who used the GFDL radiative kernels of Soden et al. (2008) to decompose the top-of-atmosphere radiative response in CMIP6 models into contributions from temperature, water vapor, surface albedo, and clouds. Within this framework, greenhouse-gas-driven cloud feedback is defined as the regression slope of the cloud radiative response against the global-mean surface temperature anomaly in the abrupt-4xCO2 experiment. In historical simulations, however, the total cloud radiative response reflects the combined influence of surface warming and aerosol–cloud interactions. Following Soden and Chung (2017), C. Wang et al. (2021) estimate the aerosol-mediated cloud radiative response (ΔR_c^{aer}, W m^{-2}) as the residual obtained after removing the temperature-driven cloud response ($\alpha_{1pctCO2} \cdot \Delta\overline{T_s}$) from the total historical cloud radiative response (ΔR_c^{tot}, W m^{-2}) :

https://doi.org/10.5194/egusphere-2026-4942
Preprint. Discussion started: 19 August 2026

$$\Delta R_c^{aer} = \Delta R_c^{tot} - \alpha_{1pctCO2} \cdot \Delta \overline{T_s} \quad (1)$$

Where $\Delta \overline{T_s}$(K) is the global-mean surface temperature anomaly, and $\alpha_{1pctCO2}$(W $m^{-2}K^{-1}$) is the normalized cloud radiative response parameter derived from the corresponding 1pctCO2 experiment. C. Wang et al. (2021) emphasize that this aerosol-mediated term encompasses both direct aerosol–cloud microphysical effects and non-local cloud changes induced by aerosol-driven adjustments in large-scale circulation, and should therefore not be interpreted as a purely local aerosol microphysical signal. They further demonstrate that estimates obtained via this residual approach are consistent with those derived from aerosol-only fixed-SST experiments and are strongly correlated with aerosol-cooling estimates obtained independently using the approximate partial radiative perturbation (APRP) method.

2.3 Aerosol Effective Radiative Forcing Decomposition

As an independent diagnostic of aerosol radiative effects, we apply the aerosol effective radiative forcing decomposition of Zelinka et al. (2023), which is based on the approximate partial radiative perturbation (APRP) technique. This method estimates shortwave aerosol effective radiative forcing directly from standard monthly model output, without requiring additional aerosol-free radiation calls. It is therefore suitable for comparing TaiESM1 with other CMIP6 models using a consistent diagnostic framework.

In this study, the APRP-based analysis is applied only to shortwave radiation. We use it to quantify the relative contributions of aerosol–radiation interactions (ERFari) and aerosol-cloud interactions (ERFaci) to TaiESM1's aerosol-related radiative response and to determine whether the dominant cooling pathway arises from direct aerosol–radiation effects or cloud-mediated processes. The decomposition also allows the cloud-mediated component to be linked to the radiative pathways identified in the cloud radiative kernel analysis, particularly the role of low- and middle-level cloud changes in producing negative shortwave cloud radiative anomalies.

Because the APRP decomposition and the cloud radiative kernel analysis diagnose different quantities, their results are interpreted as complementary rather than directly interchangeable. The kernel method diagnoses the historical cloud radiative response and its aerosol-mediated component, whereas the APRP-based method partitions the shortwave aerosol radiative effect into ERFari and ERFaci components. Consistency between the two diagnostics therefore provides process-level evidence that TaiESM1's historical aerosol-related cooling is primarily cloud-mediated and shortwave in nature.

3 Results

3.1 Simulated aerosol and cloud responses in TaiESM1

The differences among the three experimental pairs (Fig. 1) reveal distinct aerosol-, greenhouse

https://doi.org/10.5194/egusphere-2026-4942
Preprint. Discussion started: 19 August 2026

gas-, and total forcing signatures in TaiESM1. Here, historical – piControl is interpreted as the total historical response, historical – piNTCF as the aerosol-related component, and piNTCF – piControl as the greenhouse-gas-dominated component.

The total aerosol optical depth (AOD) response (historical – piControl; Fig. 1, top row) exhibits positive anomalies concentrated over major aerosol source regions, including East Asia, South Asia, the Middle East, and parts of North America, with larger amplitudes in JJA than in DJF. The aerosol-related component (historical – piNTCF; Fig. 1, middle row) displays a broadly similar spatial structure but with a weaker global-mean magnitude, indicating that the bulk of the AOD signal originates from Asian source regions and their downwind pathways. By contrast, the greenhouse-gas-dominated component (piNTCF – piControl; Fig. 1, bottom row) shows only weak AOD changes, confirming that the associated cloud and radiative responses in this contrast arise primarily from greenhouse-gas-driven climate adjustments rather than from direct changes in aerosol loading.

The simulated cloud responses depend strongly on cloud altitude. In the aerosol-related component (historical – piNTCF), low- and middle-level clouds increase over the Northern Hemisphere midlatitudes, most prominently over the North Pacific, North Atlantic, Eurasia, and the outflow regions downwind of major emission sources. These increases coincide spatially with negative shortwave cloud radiative effect (SWCF) anomalies (Fig. 2a), particularly over the North Pacific and adjacent outflow regions, consistent with enhanced shortwave reflection by low- and middle-level clouds. This correspondence between enhanced low- to mid-level cloud fraction and negative SWCF is most evident in JJA, when both aerosol loading and the associated cloud response are strongest. In contrast, high-level cloud shows a more heterogeneous spatial pattern that does not closely track the SWCF anomalies, suggesting that the shortwave cooling signal is primarily governed by changes in low- and middle-level cloud fraction rather than by changes in high-level cloud. The longwave cloud radiative effect (LWCF; Fig. 2b) response is weaker and spatially more heterogeneous than the SWCF response. In the aerosol-related component, localized positive LWCF anomalies appear over parts of the tropics and convectively active regions, coinciding with changes in middle- and high-level cloud fraction. These positive anomalies are not spatially coherent, however, and are partly offset by negative anomalies elsewhere. This suggests that the radiative signature of aerosol-related cloud changes in TaiESM1 is dominated by shortwave rather than longwave cooling.

The greenhouse-gas-dominated component (piNTCF – piControl) presents a contrasting cloud–radiation relationship. Relative to the aerosol-related component, low- and middle-levels generally decrease across broad midlatitude and storm-track regions, whereas high-levels exhibit a more mixed response, with localized increases at high latitudes and in parts of the tropics. The corresponding SWCF pattern is spatially complex and partly reflects the reduction in low- and middle-level cloud reflectivity. The associated LWCF response also differs qualitatively from that of the aerosol-related component, indicating that greenhouse-gas-driven cloud adjustments partially offset the aerosol-induced cloud radiative effect at the global scale.

https://doi.org/10.5194/egusphere-2026-4942
Preprint. Discussion started: 19 August 2026

Taken together, these results demonstrate that the total historical cloud radiative response in TaiESM1 cannot be attributed to a single forcing mechanism. The aerosol-related component exerts its strongest influence through increases in low- and middle-level cloud fraction and the associated negative SWCF anomalies over Northern Hemisphere aerosol outflow regions. In contrast, the greenhouse-gas-dominated component drives more broadly distributed cloud redistribution and radiative adjustment. The total historical response therefore reflects a spatially dependent compensation between aerosol-induced cloud brightening and greenhouse-gas-driven cloud changes, with the most pronounced aerosol–cloud signal concentrated over Northern Hemisphere midlatitude oceans and polluted outflow regions.

3.2 Cloud Radiative Kernel Diagnostics

Figure 3 diagnoses the cloud radiative response of TaiESM1 using the cloud radiative kernel framework of C. Wang et al. (2021). The results reveal substantial differences in the total cloud radiative response and the aerosol-mediated cloud radiative response among the three forcing contrasts, despite an essentially identical cloud feedback pattern across experiments. For the fully coupled historical contrast, defined as historical - piControl (Fig. 3a), the total cloud radiative response is strongly negative, with a global mean of −2.08 W m^{-2}. The aerosol-mediated cloud radiative response is even more negative, reaching −2.24 W m^{-2}. The strongest negative anomalies are concentrated over Northern Hemisphere marine regions, particularly the North Pacific and North Atlantic, as well as oceanic regions downstream of major continental aerosol source areas. This spatial structure is consistent with the AOD diagnostics presented earlier (Fig. 1), in which enhanced aerosol loading is concentrated over East Asia, South Asia, and other anthropogenic source regions, and with the cloud-fraction diagnostics, which show increases in low- and middle-level cloud fraction over the same downstream marine regions. The collocation of the negative cloud radiative response with enhanced low- and middle-level clouds, together with negative SWCF anomalies (Fig. 2), indicates that the dominant radiative pathway is shortwave cooling associated with these clouds. By contrast, LWCF changes are weaker and less spatially coherent, suggesting that the net negative cloud radiative response is governed primarily by the shortwave component.

The difference between AerosolOnly and piControl (Fig. 3b) shows that aerosol-forced response under the pre-industrial background state can produce a substantial negative cloud radiative response in TaiESM1. The total cloud radiative response is −1.77 W m^{-2}, and the aerosol-mediated cloud radiative response is −1.15 W m^{-2}. The spatial pattern shares several features with the historical and piControl contrast (Fig. 3a), including pronounced negative anomalies over Northern Hemisphere marine outflow regions, but the aerosol-mediated response is weaker in magnitude than in the fully coupled historical contrast. This discrepancy indicates that aerosol forcing imposed on a pre-industrial background state does not fully reproduce the magnitude of the historical response, suggesting that the background climate state, including SST-constrained circulation and cloud-regime distribution,

https://doi.org/10.5194/egusphere-2026-4942
Preprint. Discussion started: 19 August 2026

modulates the amplitude and spatial organization of the diagnosed aerosol-mediated response. The difference between piNTCF and piControl (Fig. 3c) shows behavior distinct from that of the historical and AerosolOnly contrasts. The total cloud radiative response is only weakly negative, at −0.20 W m^{-2}, whereas the aerosol-mediated cloud radiative response remains substantially negative, at −1.03 W m^{-2}. This indicates that the piNTCF–piControl contrast still produces a non-negligible aerosol-mediated cloud cooling, but its magnitude is weaker than that diagnosed in the historical and AerosolOnly contrasts. The weak total response results from compensation between the negative aerosol-mediated component and the positive temperature-mediated cloud feedback contribution. Because anthropogenic aerosol perturbations are not the primary forcing pathway in the piNTCF–piControl contrast, this response is interpreted mainly as a background cloud-radiative adjustment associated with changes in biogenic emissions, circulation, and thermodynamic state rather than as a direct anthropogenic aerosol-forcing signal. The cloud feedback pattern is nearly identical across the three forcing contrasts, with a global-mean value of approximately +0.84 W m^{-2} K^{-1}. It is therefore shown only once (Fig. 3d). The diagnosed positive global-mean cloud feedback indicates that TaiESM1 tends to amplify warming through cloud-radiative adjustments.

Taken together with the AOD, SWCF, LWCF, and low-, middle-, and high-level clouds, the diagnostics presented in Section 3.1 indicate that TaiESM1's aerosol-mediated cloud cooling is primarily associated with changes in low- and middle-level clouds and their shortwave radiative effects. The high-cloud response is more spatially heterogeneous and does not align as closely with the strongest negative SWCF anomalies. The cloud radiative kernel diagnostics therefore point to a shortwave-dominated, aerosol-related cloud response concentrated over Northern Hemisphere marine outflow regions.

3.3 Aerosol effective radiative forcing

To further identify the radiative origin of the aerosol-related cooling diagnosed in Sect. 3.2, we apply the APRP-based aerosol effective radiative forcing decomposition following Zelinka et al. (2023). Figure 4 presents the spatial distribution of shortwave ERF components for the historical and piControl contrast, including the total SW ERF(ari+aci), SW ERF(ari), and SW ERF(aci). Figure 5 further summarizes the corresponding global-mean decomposition into aerosol–radiation and aerosol–cloud contributions, and further into scattering, absorption, and cloud-amount components.

The spatial pattern of SW ERF(ari+aci) in Fig. 4 is dominated by negative anomalies over Northern Hemisphere marine regions, particularly the North Pacific and North Atlantic. This pattern closely resembles the negative total and aerosol-mediated cloud radiative response diagnosed by the cloud radiative kernel analysis in Sect. 3.2. The strongest negative shortwave forcing occurs over regions where enhanced aerosol loading and increases in low- and middle-level cloud fraction were also identified, indicating that the strong negative cloud radiative response in TaiESM1 is expressed primarily through shortwave aerosol–cloud forcing.

https://doi.org/10.5194/egusphere-2026-4942
Preprint. Discussion started: 19 August 2026

The decomposition in Fig. 4 shows that the shortwave forcing pattern is governed mainly by SW ERF(aci). TaiESM1 produces a global-mean SW ERF(ari+aci) of approximately −2.34 W m^{-2}, of which SW ERF(aci) accounts for about −2.00 W m^{-2}. By contrast, SW ERF(ari) is much weaker, at approximately −0.34 W m^{-2} (Fig. 5), with a more spatially diffuse pattern. The large shortwave aerosol cooling in TaiESM1 therefore cannot be attributed primarily to direct aerosol–radiation interactions; instead, it is mainly associated with aerosol–cloud interactions. The global-mean decomposition in Fig. 5 further clarifies the processes underlying this shortwave response. For SW ERF(ari), aerosol scattering contributes a negative forcing of approximately −0.72 W m^{-2}, partly offset by aerosol absorption of about +0.38 W m^{-2}, yielding a comparatively weak net SW ERF(ari) of −0.34 W m^{-2}. For SW ERF(aci), the cloud-scattering component dominates, contributing approximately −2.14 W m^{-2}, whereas the cloud-amount term is small and positive, at about +0.12 W m^{-2}. This indicates that the shortwave aerosol–cloud forcing in TaiESM1 is driven primarily by aerosol-induced changes in cloud optical scattering rather than by an increase in cloud amount alone.

Together with the kernel-based results in Sect. 3.2, these diagnostics indicate that TaiESM1's historical aerosol-related cloud response is controlled mainly by aerosol-induced changes in cloud reflectivity over Northern Hemisphere marine outflow regions. The broader inter-model implications of this cloud-mediated shortwave response are discussed in Sect. 4.1.

4 Discussion

4.1 Strong cloud-mediated aerosol cooling in TaiESM1

The cloud radiative kernel analysis (Sect. 3.2) and the APRP-based aerosol ERF decomposition (Sect. 3.3) diagnose different aspects of aerosol–cloud–radiation coupling, but together they indicate that TaiESM1 exhibits a strong cloud-mediated aerosol cooling. The kernel analysis shows a pronounced negative aerosol-mediated cloud radiative response in the historical simulation, whereas the APRP decomposition indicates that ERFaci rather than ERFari dominates the shortwave aerosol forcing. The two quantities should not be compared term-by-term, since the former represents a kernel-derived historical cloud radiative response and the latter an APRP-derived shortwave aerosol effective radiative forcing component; their qualitative agreement is nevertheless physically informative, as both diagnostics independently identify cloud-mediated shortwave cooling as the dominant aerosol-related response in TaiESM1.

The ERFari–ERFaci phase space across a selected set of CMIP6 models (Fig. 6) further clarifies the origin of TaiESM1's aerosol forcing. TaiESM1 lies near the strong-ERFaci end of the model sample, with ERFaci of approximately −2.0 W m^{-2} and a comparatively weak ERFari of about −0.3 W m^{-2}. This places TaiESM1 close to MRI in terms of strong cloud-mediated forcing, while CESM2 and NorESM2 also exhibit substantial negative ERFaci but with markedly different ERFari characteristics. By contrast, MPI, GFDL, CanESM5, and IPSL show much weaker ERFaci, with values close to zero or, in the case of IPSL, slightly positive. This comparison indicates that TaiESM1's strong aerosol

https://doi.org/10.5194/egusphere-2026-4942
Preprint. Discussion started: 19 August 2026

forcing cannot be attributed primarily to clear-sky aerosol–radiation interactions and instead reflects an enhanced cloud-mediated response.

A similar conclusion emerges from comparing the APRP-derived ERFaci with the kernel-derived aerosol-mediated cloud radiative response (Fig. 7). Across the CMIP6 models, more negative aerosol-mediated cloud radiative responses generally correspond to more negative ERFaci, although the relationship is not one-to-one. TaiESM1 lies at the strong-response end of both diagnostics, exhibiting the most negative aerosol-mediated cloud radiative response among the sampled models together with one of the strongest negative ERFaci values. MRI likewise shows strong ERFaci but a weaker aerosol-mediated response than TaiESM1, whereas CanESM5, GFDL, and MPI show comparatively weak responses in both diagnostics. IPSL departs from the overall inter-model relationship, combining a moderately negative aerosol-mediated response with a weak, slightly positive ERFaci, suggesting that its historical cloud radiative response may involve processes not fully captured by the APRP-defined shortwave cloud forcing alone.

The TS shading in Figs. 6 and 7 provides further context for the potential climatic implications of the aerosol–cloud diagnostics. Models with weaker cloud-mediated aerosol cooling, such as IPSL, CanESM5, and MPI, generally show larger TS values, whereas TaiESM1 is located near the strong negative end of both ERFaci and the kernel-derived aerosol-mediated cloud radiative response and is associated with one of the smaller TS values among the sampled models. This distribution is broadly consistent with the compensation mechanism proposed by Wang et al. (2021), in which stronger aerosol-induced cloud cooling can offset part of the greenhouse-gas-induced warming over the historical period. However, the relationship is not one-to-one. CESM2, for example, exhibits substantial negative ERFaci but a relatively large TS value, indicating that the realized warming amplitude also depends on greenhouse-gas forcing, cloud feedback strength, ERFari, ocean heat uptake, and circulation adjustment. Therefore, TS should be interpreted as an integrated climate response modulated by aerosol–cloud interactions, rather than as a direct measure of the strength of aerosol–cloud interactions alone.

Together, these results suggest that aerosol–cloud coupling is a central control on TaiESM1's historical cloud radiative response. Future model development should therefore prioritize processes that regulate aerosol activation, cloud droplet number concentration, droplet effective radius, cloud optical depth, and adjustments in low- to middle-level clouds. Particular attention should be given to cloud–radiation coupling, since the dominant APRP signal arises from cloud scattering rather than from cloud amount. Improving the representation of cloud amount alone would therefore be insufficient; the key question is whether TaiESM1 correctly represents how aerosol perturbations modify cloud optical properties and shortwave reflection.

4.2 Ocean-mediated adjustment of aerosol-related cloud radiative responses

Figure 8 examines the role of ocean coupling by comparing the prescribed-SST historical

https://doi.org/10.5194/egusphere-2026-4942
Preprint. Discussion started: 19 August 2026

response (histSST-piControl) and the interactive-ocean residual (historical - histSST). The difference between historical and piControl (Fig. 3a) and the difference between histSST and piControl (Fig. 8a) exhibit very similar spatial patterns for both the total and aerosol-mediated cloud radiative responses, with global-mean total cloud radiative responses of −2.08 and −2.00 W m^{-2}, respectively, and aerosol-mediated cloud radiative responses of −2.24 and −2.22 W m^{-2}. In both contrasts, negative anomalies dominate over Northern Hemisphere marine regions, particularly the North Pacific and North Atlantic, with additional signals over subtropical eastern-ocean cloud regimes. This close agreement indicates that the prescribed-SST historical experiment captures most of the large-scale historical cloud radiative response simulated by TaiESM1.

The AOD and cloud-fraction diagnostics further support this interpretation. The AOD changes due to fully coupled historical response (historical – piControl, Fig. 1) and prescribed-SST historical response (histSST – piControl, Fig. 9) are highly similar, with global-mean increases of 0.019 and 0.018, respectively. Both contrasts show enhanced aerosol loading over major anthropogenic source regions, including East Asia, South Asia, and parts of the Northern Hemisphere midlatitudes. By contrast, the AOD difference between historical and histSST is very small, with a global mean of only 0.002, and shows no coherent large-scale aerosol-loading pattern. This indicates that differences in aerosol burden do not primarily drive the difference between the coupled and prescribed-SST historical simulations.

The differences in cloud fraction indicate that the prescribed-SST historical response captures much of the large-scale cloud adjustment, but that the sensitivity to interactive ocean coupling varies with cloud altitude. For high clouds, the fully coupled historical response and prescribed-SST historical response show broadly similar global-mean decreases of approximately −0.30% and −0.28%, respectively, while the coupled-ocean adjustment is small, at −0.02%. This indicates that the high-cloud response is largely associated with the prescribed historical SST and forcing background, rather than with additional interactive ocean adjustment. For middle clouds, however, the coupled-ocean adjustment is more evident. The fully coupled historical response shows a global-mean decrease of about −0.16%, while the prescribed-SST historical response accounts for −0.08% and the historical − histSST residual contributes an additional −0.08%. This near-equal partitioning suggests that interactive ocean coupling can substantially modify the middle-cloud response, even though its effect on the global-mean radiative budget remains much smaller than the prescribed-SST historical signal. For low clouds, the prescribed-SST historical response shows a global-mean increase of +0.17%, whereas the coupled-ocean adjustment is slightly negative, at −0.03%. Thus, interactive ocean coupling does not reinforce the low-cloud increase; rather, it weakly offsets the prescribed-SST low-cloud response and redistributes low-cloud changes regionally.

Overall, Fig. 9 indicates that the coupled-ocean impacts primarily on the vertical redistribution of cloud fraction, particularly for middle clouds, with a weaker compensating adjustment in low clouds and only a small residual in high clouds. This supports the interpretation that interactive ocean coupling

https://doi.org/10.5194/egusphere-2026-4942
Preprint. Discussion started: 19 August 2026

modulates the regional and vertical structure of cloud responses, rather than controlling the large-scale aerosol loading or the dominant global-mean shortwave cooling.

The SWCF and LWCF diagnostics (Fig. 10) further clarify this point. The SWCF changes due to fully coupled historical response and prescribed-SST historical response are nearly identical in the global mean, at −1.74 and −1.72 W m^{-2}, respectively, and show very similar negative anomalies over Northern Hemisphere marine regions. By contrast, the coupled-ocean adjustment in SWCF is close to zero globally (about −0.02 W m^{-2}) and is spatially weak. The LWCF response follows the same hierarchy, albeit with smaller amplitudes: the fully coupled historical response and prescribed-SST historical response contrasts yield global means of −0.34 and −0.28 W m^{-2}, respectively, whereas the coupled-ocean adjustment is only −0.06 W m^{-2}. These results indicate that the historical cloud radiative response is dominated by the common prescribed-SST background response, particularly through shortwave cloud radiative changes, while the additional effect of interactive ocean coupling remains much smaller in the global mean.

The difference between historical and histSST simulations (Fig. 8b) nevertheless shows that this coupled-ocean residual is not spatially uniform. Weak negative anomalies remain over parts of the North Pacific, and clearer regional signals appear over the eastern and southeastern Pacific off South America. These features occur in marine cloud regimes, where cloud properties are sensitive to SST, lower-tropospheric stability, subsidence, and boundary-layer structure. However, the present diagnostics alone do not identify which of these processes controls the regional residual, and the signals over the eastern and southeastern Pacific should therefore be interpreted conservatively as evidence of a regionally coupled ocean-atmosphere cloud adjustment, rather than as direct proof of a specific SST-feedback mechanism.

Overall, Figure 8 and the accompanying diagnostics of AOD, cloud fraction, SWCF, and LWCF (Figs. 9 and 10) indicate that ocean coupling plays a secondary but regionally relevant role in TaiESM1's aerosol-related cloud radiative response. The dominant historical signal is already present in the prescribed-SST historical simulation and is closely aligned with the fully coupled historical response. The additional effect of interactive ocean coupling is small in the global-mean radiative budget, especially for SWCF, but it can reorganize cloud responses regionally and alter the vertical distribution of cloud fraction, particularly for middle-level clouds.

5 Conclusion

This study has combined cloud radiative kernel diagnostics (C. Wang et al., 2021) with an APRP-based decomposition of aerosol effective radiative forcing (Zelinka et al., 2023) to characterize the aerosol–cloud–radiation coupling simulated by TaiESM1 over the historical period. Three main conclusions emerge from this process-oriented analysis.

First, TaiESM1 simulates a strongly negative total cloud radiative response over the historical period (historical-piControl: −2.08 W m^{-2}), of which the aerosol-mediated component accounts for the majority of the signal (−2.24 W m^{-2}), despite positive global-mean cloud feedback of approximately +0.84 W m^{-2} K^{-1}. This total historical response therefore reflects a spatially dependent compensation between aerosol-induced cloud brightening and greenhouse-gas-driven cloud adjustments, with the strongest aerosol-related cooling concentrated over Northern Hemisphere marine outflow regions such as the North Pacific and North Atlantic, consistent across AOD, cloud-fraction, and cloud radiative kernel diagnostics.

Second, the APRP decomposition demonstrates that this aerosol-related cooling is predominantly shortwave and cloud-mediated. TaiESM1 produces a global-mean SW ERF(ari+aci) of approximately −2.34 W m^{-2}, of which SW ERF(aci) contributes about −2.00 W m^{-2}, compared with a much weaker SW ERF(ari) of approximately −0.34 W m^{-2}. Within the aerosol–cloud interaction term, the response is governed primarily by cloud scattering (−2.14 W m^{-2}) rather than by cloud-amount changes (+0.12 W m^{-2}), indicating that aerosol-induced changes in cloud optical properties, rather than cloud coverage alone, control TaiESM1's historical shortwave aerosol forcing. In the inter-model context, TaiESM1 lies at the strong-ERFaci end of the selected CMIP6 model sample examined here, with a cloud-mediated forcing comparable to or exceeding that of MRI and CESM2, and substantially stronger than that of MPI, GFDL, CanESM5, and IPSL, confirming that TaiESM1's aerosol forcing is disproportionately controlled by cloud-mediated rather than clear-sky aerosol–radiation processes.

Third, interactive ocean coupling plays a secondary and regional role in shaping this response. The prescribed-SST historical experiment reproduces most of the magnitude and spatial pattern of the fully coupled historical response. In contrast, the residual ocean coupling effect (historical – histSST) is weaker in the global mean (total cloud radiative response of -0.08 W m^{-2}), but it modifies the regional distribution of the response, particularly over the North Pacific and the Southeast Pacific. This result indicates that the aerosol-forced cloud response in TaiESM1 is primarily a direct radiative and microphysical effect, with ocean-mediated circulation and SST feedbacks acting as secondary regional modulators rather than the primary drivers.

Taken together, these findings identify aerosol-induced changes in low- and middle-level cloud reflectivity, and specifically cloud optical scattering, as the key process underlying TaiESM1's historical aerosol-related cloud cooling. Future development of TaiESM1 should therefore prioritize the representation of aerosol activation, cloud droplet number concentration, droplet effective radius, and cloud optical depth, as well as the cloud-regime-dependent processes governing adjustments in low- and middle-level clouds over Northern Hemisphere marine outflow regions. Because the piNTCF-based diagnostic does not cleanly isolate anthropogenic aerosol forcing in TaiESM1, future work should also consider complementary experimental designs to more robustly separate anthropogenic aerosol effects from circulation- and emission-driven variability.

Acknowledgment

The National Science and Technology Council supported this work. We also thank the National Center for High-performance Computing for providing computational resources.

Funding

The National Science and Technology Council supported this work through grant numbers NSTC-114-2111-M-001 -005 -, NSTC-115-2111-M-001 -001 -, NSTC-115-2119-M-001 -006 -, NSTC-115-2119-M-002 -014-.

https://doi.org/10.5194/egusphere-2026-4942
Preprint. Discussion started: 19 August 2026

References

Ackerman, A. S., Toon, O. B., Taylor, J. P., Johnson, D. W., Hobbs, P. V., & Ferek, R. J. (2000). Effects of Aerosols on Cloud Albedo: Evaluation of Twomey's Parameterization of Cloud Susceptibility Using Measurements of Ship Tracks. *Journal of the Atmospheric Sciences*, *57*(16), 2684–2695. https://doi.org/https://doi.org/10.1175/1520-0469(2000)057<2684:EOAOCA>2.0.CO;2

Albrecht, B. A. (1989). Aerosols, Cloud Microphysics, and Fractional Cloudiness. *Science*, *245*(4923), 1227–1230. https://doi.org/doi:10.1126/science.245.4923.1227

Bellouin, N., Quaas, J., Gryspeerdt, E., Kinne, S., Stier, P., Watson-Parris, D., Boucher, O., Carslaw, K. S., Christensen, M., Daniau, A. L., Dufresne, J. L., Feingold, G., Fiedler, S., Forster, P., Gettelman, A., Haywood, J. M., Lohmann, U., Malavelle, F., Mauritsen, T.,…Stevens, B. (2020). Bounding Global Aerosol Radiative Forcing of Climate Change. *Rev Geophys*, *58*(1), e2019RG000660. https://doi.org/10.1029/2019rg000660

Chen, J.-P., Tsai, I., & Lin, Y.-C. (2013). A statistical–numerical aerosol parameterization scheme. *Atmospheric Chemistry and Physics*, *13*(20), 10483–10504.

Collins, W. J., Lamarque, J.-F., Schulz, M., Boucher, O., Eyring, V., Hegglin, M. I., Maycock, A., Myhre, G., Prather, M., & Shindell, D. (2017). AerChemMIP: quantifying the effects of chemistry and aerosols in CMIP6. *Geoscientific Model Development*, *10*(2), 585–607.

Eyring, V., Bony, S., Meehl, G. A., Senior, C. A., Stevens, B., Stouffer, R. J., & Taylor, K. E. (2016). Overview of the Coupled Model Intercomparison Project Phase 6 (CMIP6) experimental design and organization. *Geoscientific Model Development*, *9*(5), 1937–1958.

Hurrell, J. W., Holland, M. M., Gent, P. R., Ghan, S., Kay, J. E., Kushner, P. J., Lamarque, J.-F., Large, W. G., Lawrence, D., & Lindsay, K. (2013). The community earth system model: a framework for collaborative research. *Bulletin of the American Meteorological Society*, *94*(9), 1339–1360.

Lee, W. L., Liou, K. N., Wang, C. c., Gu, Y., Hsu, H. H., & Li, J. L. F. (2019). Impact of 3-D radiation-topography interactions on surface temperature and energy budget over the Tibetan Plateau in winter. *Journal of Geophysical Research: Atmospheres*, *124*(3), 1537–1549.

Lee, W. L., Wang, Y. C., Shiu, C. J., Tsai, I., Tu, C. Y., Lan, Y. Y., Chen, J. P., Pan, H. L., & Hsu, H. H. (2020). Taiwan Earth System Model Version 1: description and evaluation of mean state. *Geosci. Model Dev.*, *13*(9), 3887–3904. https://doi.org/10.5194/gmd-13-3887-2020

Park, C., Soden, B. J., Kramer, R. J., L'Ecuyer, T. S., & He, H. (2025). Observational constraints suggest a smaller effective radiative forcing from aerosol–cloud interactions. *Atmospheric Chemistry and Physics*, *25*(13), 7299–7313.

Sherwood, S. C., Webb, M. J., Annan, J. D., Armour, K. C., Forster, P. M., Hargreaves, J. C., Hegerl, G., Klein, S. A., Marvel, K. D., Rohling, E. J., Watanabe, M., Andrews, T., Braconnot, P., Bretherton, C. S., Foster, G. L., Hausfather, Z., von der Heydt, A. S., Knutti, R., Mauritsen, T.,…Zelinka, M. D. (2020). An Assessment of Earth's Climate Sensitivity Using Multiple Lines of Evidence. *Rev Geophys*, *58*(4), e2019RG000678. https://doi.org/10.1029/2019rg000678

https://doi.org/10.5194/egusphere-2026-4942
Preprint. Discussion started: 19 August 2026

Shiu, C. J., Wang, Y. C., Hsu, H. H., Chen, W. T., Pan, H. L., Sun, R., Chen, Y. H., & Chen, C. A. (2021). GTS v1.0: a macrophysics scheme for climate models based on a probability density function. *Geosci. Model Dev.*, *14*(1), 177–204. https://doi.org/10.5194/gmd-14-177-2021

Smith, C. J., Kramer, R. J., Myhre, G., Alterskjær, K., Collins, W., Sima, A., Boucher, O., Dufresne, J. L., Nabat, P., Michou, M., Yukimoto, S., Cole, J., Paynter, D., Shiogama, H., O'Connor, F. M., Robertson, E., Wiltshire, A., Andrews, T., Hannay, C.,…Forster, P. M. (2020). Effective radiative forcing and adjustments in CMIP6 models. *Atmos. Chem. Phys.*, *20*(16), 9591–9618. https://doi.org/10.5194/acp-20-9591-2020

Soden, B., & Chung, E.-S. (2017). The large-scale dynamical response of clouds to aerosol forcing. *Journal of Climate*, *30*(21), 8783–8794.

Soden, B. J., Held, I. M., Colman, R., Shell, K. M., Kiehl, J. T., & Shields, C. A. (2008). Quantifying climate feedbacks using radiative kernels. *Journal of Climate*, *21*(14), 3504–3520.

Tsai, I.-C., Yang, S.-W., Shiu, C.-J., Chen, Y.-Y., Chen, C.-A., Lee, W.-L., & Hsu, H.-H. (2024). Aerosol impacts on the East Asian winter monsoon: Insights from TaiESM1 and CMIP6 simulations. *International Journal of Climatology*, *44*(9), 2816–2832. https://doi.org/10.1002/joc.8483

Tsai, I. C., Shiu, C.-J., Chen, C.-A., Hsu, H.-H., Mao, Y.-Y., & Wang, W.-C. (2025). Investigating the causes of cloud diurnal variation biases in global climate models using the TaiESM1. *Atmospheric Research*, *316*, 107976. https://doi.org/10.1016/j.atmosres.2025.107976

Twomey, S. (1974). Pollution and the planetary albedo. *Atmospheric Environment (1967)*, *8*(12), 1251–1256. https://doi.org/10.1016/0004-6981(74)90004-3

Twomey, S. (1977). The influence of pollution on the shortwave albedo of clouds. *J. atmos. Sci*, *34*, 1149–1152.

Wall, C. J., Storelvmo, T., & Possner, A. (2023). Global observations of aerosol indirect effects from marine liquid clouds. *Atmospheric Chemistry and Physics*, *23*(20), 13125–13141.

Wang, C., Soden, B. J., Yang, W., & Vecchi, G. A. (2021). Compensation Between Cloud Feedback and Aerosol-Cloud Interaction in CMIP6 Models. *Geophysical Research Letters*, *48*(4), e2020GL091024. https://doi.org/10.1029/2020GL091024

Wang, Y.-C., Hsu, H.-H., Chen, C.-A., Tseng, W.-L., Hsu, P.-C., Lin, C.-W., Chen, Y.-L., Jiang, L.-C., Lee, Y.-C., Liang, H.-C., Chang, W.-M., Lee, W.-L., & Shiu, C.-J. (2021). Performance of the Taiwan Earth System Model in Simulating Climate Variability Compared With Observations and CMIP6 Model Simulations. *Journal of Advances in Modeling Earth Systems*, *13*(7), e2020MS002353. https://doi.org/10.1029/2020MS002353

Wang, Y. C., Pan, H. L., & Hsu, H. H. (2015). Impacts of the triggering function of cumulus parameterization on warm-season diurnal rainfall cycles at the Atmospheric Radiation Measurement Southern Great Plains site. *Journal of Geophysical Research: Atmospheres*, *120*(20), 10,681–610,702.

https://doi.org/10.5194/egusphere-2026-4942
Preprint. Discussion started: 19 August 2026

Zelinka, M. D., Myers, T. A., McCoy, D. T., Po-Chedley, S., Caldwell, P. M., Ceppi, P., Klein, S. A., & Taylor, K. E. (2020). Causes of Higher Climate Sensitivity in CMIP6 Models. *Geophysical Research Letters*, *47*(1), e2019GL085782. https://doi.org/10.1029/2019GL085782

Zelinka, M. D., Smith, C. J., Qin, Y., & Taylor, K. E. (2023). Comparison of methods to estimate aerosol effective radiative forcings in climate models. *Atmos. Chem. Phys.*, *23*(15), 8879–8898. https://doi.org/10.5194/acp-23-8879-2023

https://doi.org/10.5194/egusphere-2026-4942
Preprint. Discussion started: 19 August 2026

Table 1. Summary of TaiESM1 experiments used in this study.

Experiment	Configuration	Diagnostic role
piControl	Pre-industrial forcing; fully coupled ocean	Reference climate
Historical	Historical forcing; fully coupled ocean	Fully coupled historical response
histSST	Historical forcing; prescribed SST/sea ice	Prescribed-SST historical response
piNTCF	Historical forcing with NTCFs fixed at pre-industrial levels	NTCF-related contrast
AerosolOnly	Historical aerosol forcing under PI background	Aerosol-forced response

https://doi.org/10.5194/egusphere-2026-4942
Preprint. Discussion started: 19 August 2026

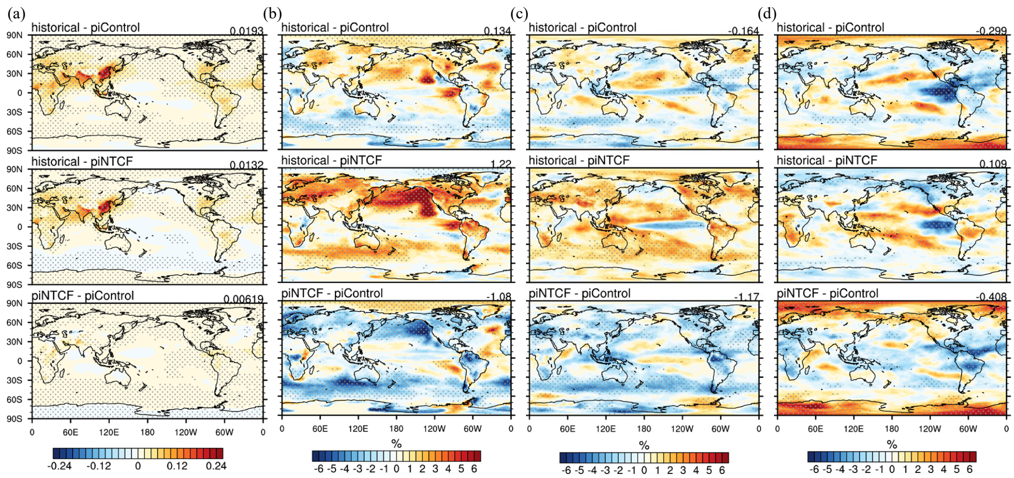

Figure 1. Annual-mean differences in (a) aerosol optical depth, (b)low-level cloud fraction, (c) middle-level cloud fraction, and (d) high-level cloud fraction (in %) among three TaiESM1 experiment pairs: historical – piControl (total historical response; top row), historical – piNTCF (aerosol-related response; middle row), and piNTCF – piControl (greenhouse-gas-dominated response; bottom row). Stippling indicates grid points where the difference is statistically significant at the 95% confidence level.

https://doi.org/10.5194/egusphere-2026-4942
Preprint. Discussion started: 19 August 2026

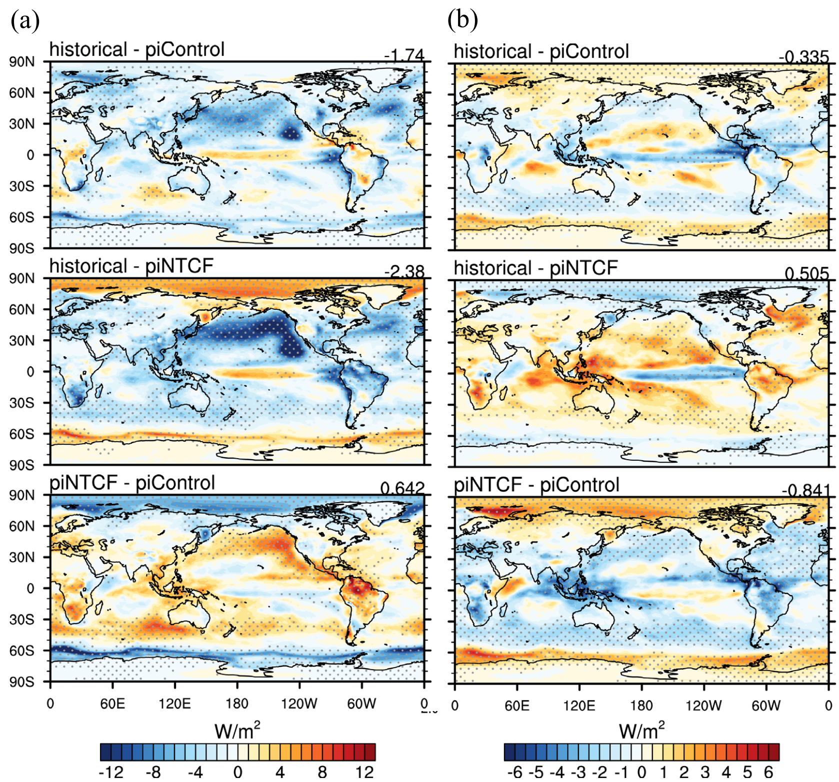

Figure 2. Annual-mean differences in (a) shortwave and (b) longwave cloud radiative effects (W m^{-2}) in TaiESM1. Differences among the three experiment pairs: historical – piControl, historical – piNTCF, and piNTCF – piControl (top to bottom). Numbers in the upper-right corner of each panel indicate global-mean differences. Stippling indicates statistical significance at the 95% confidence level.

https://doi.org/10.5194/egusphere-2026-4942
Preprint. Discussion started: 19 August 2026

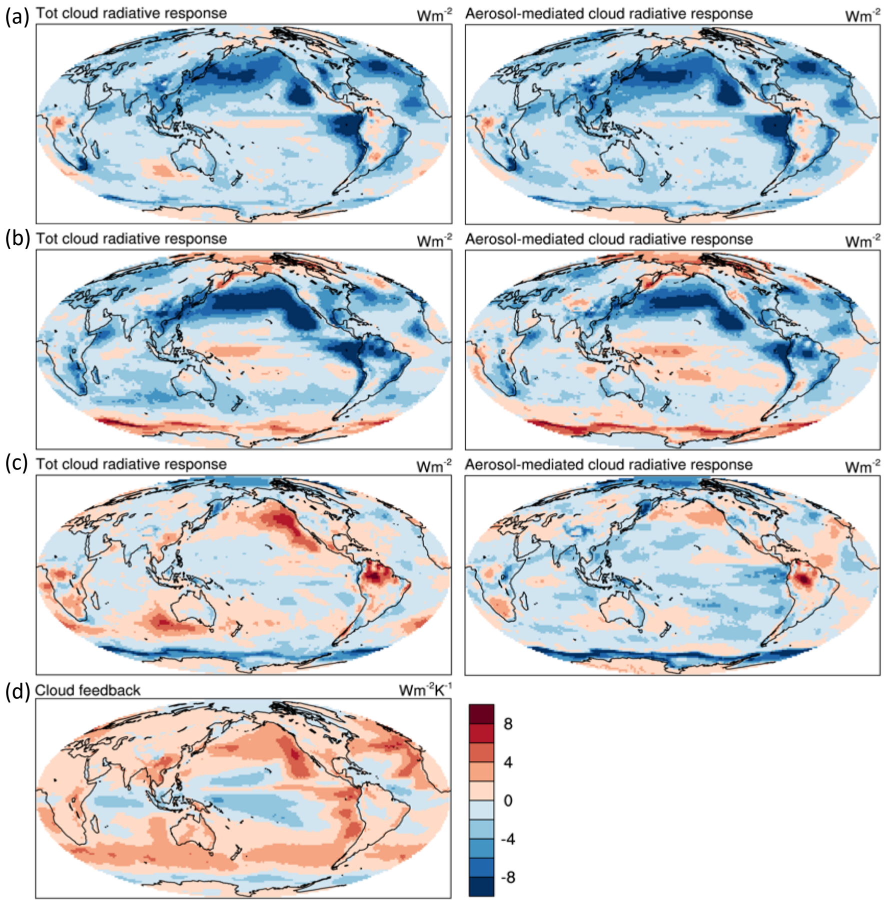

Figure 3. Cloud radiative kernel diagnostics for TaiESM1, following the framework of Wang et al. (2021). Rows show, from top to bottom, the (a) fully coupled historical contrast (historical – piControl), (b) aerosol forcing alone (AerosolOnly - piControl), and (c) the biogenic-emission- and circulation-related background response (piNTCF - piControl). For each contrast, the top row shows the total cloud radiative response (W m^{-2}) and the bottom row shows the aerosol-mediated cloud radiative response (W m^{-2}), obtained as the residual after removing the temperature-driven cloud response (Section 2.2). The fourth column (d) shows the cloud feedback pattern (W m^{-2} K^{-1}), which is nearly identical across the three contrasts and is therefore presented only once as a common model property. Color shading follows the shared scale shown at right (W m^{-2} for the total and aerosol-mediated cloud radiative response panels; W m^{-2} K^{-1} for the cloud feedback panel).

https://doi.org/10.5194/egusphere-2026-4942
Preprint. Discussion started: 19 August 2026

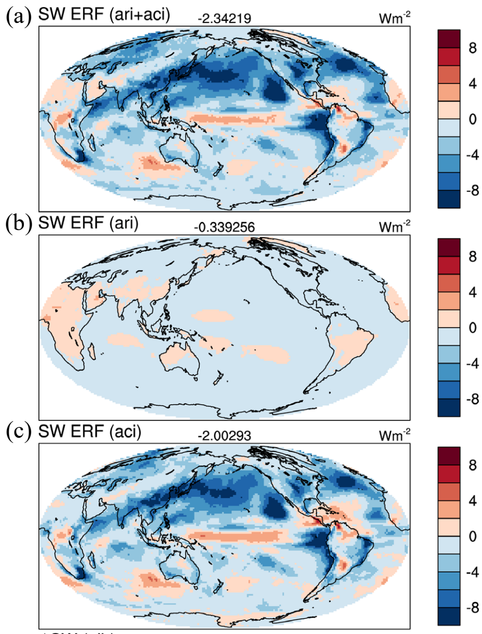

Figure 4. Spatial distribution of the shortwave aerosol effective radiative forcing (SW ERF, W m^{-2}) for the fully coupled historical response, defined as historical minus piControl (historical – piControl), decomposed following the APRP-based method of Zelinka et al. (2023) into (a) total aerosol–radiation plus aerosol–cloud interactions, SW ERF(ari+aci); (b) aerosol–radiation interactions, SW ERF(ari); and (c) aerosol–cloud interactions, SW ERF(aci). Values are computed as the difference between the last 30 years of the historical simulation and the piControl climatology. Global-mean values are given above each panel. Color shading follows the scale shown at right (W m^{-2}).

https://doi.org/10.5194/egusphere-2026-4942
Preprint. Discussion started: 19 August 2026

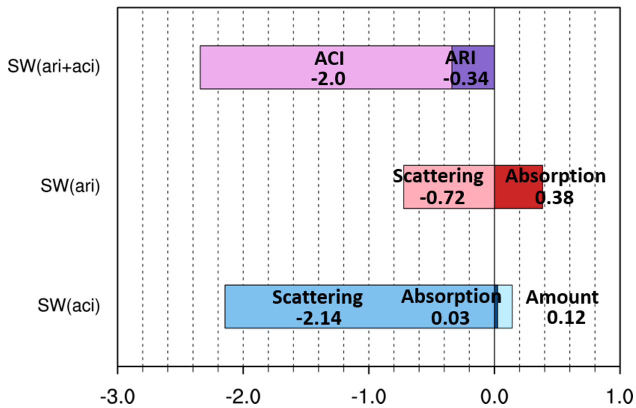

Figure 5. Global-mean aerosol effective radiative forcing (W m^{-2}) for TaiESM1, decomposed following the APRP-based method for the fully coupled historical contrast (historical – piControl). From top to bottom: the total shortwave aerosol forcing [SW(ari+aci)] is separated into aerosol–radiation interactions (ari) and aerosol–cloud interactions (aci). The middle bar decomposes SW(ari) into aerosol scattering and absorption. The bottom bar decomposes SW(aci) into cloud scattering, absorption, and cloud amount. Values are global means in W m^{-2}. Negative values indicate cooling, and positive values indicate warming. The vertical black line marks zero forcing.

https://doi.org/10.5194/egusphere-2026-4942
Preprint. Discussion started: 19 August 2026

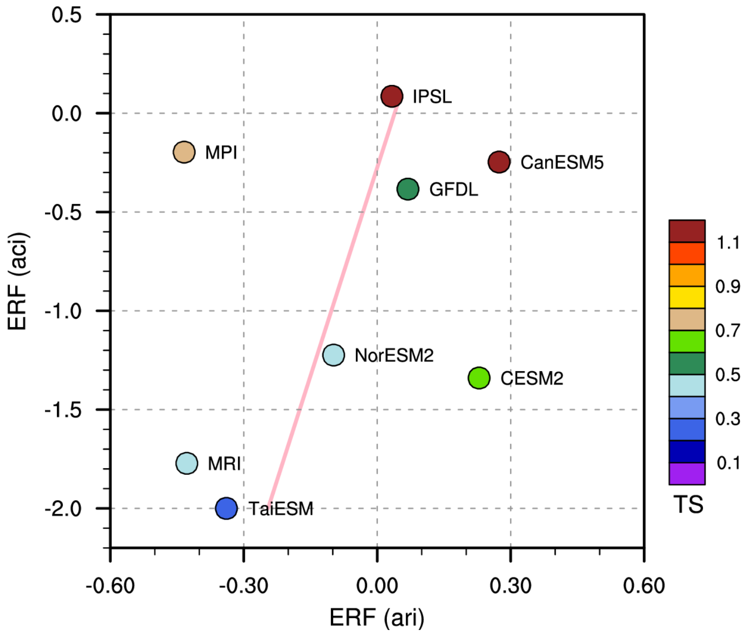

Figure 6. Inter-model comparison of APRP-derived shortwave aerosol forcing components. The scatter plot shows aerosol–radiation interactions, ERFari (W m^{-2}; x-axis), versus aerosol–cloud interactions, ERFaci (W m^{-2}; y-axis), for TaiESM1 and selected CMIP6-class models. Marker colors indicate the corresponding TS changes between historical and piControl, and the pink line denotes the linear least-squares fit across the displayed models. TaiESM1 lies at the lower-left side of the distribution, characterized by strongly negative ERFaci and moderately negative ERFari.

https://doi.org/10.5194/egusphere-2026-4942
Preprint. Discussion started: 19 August 2026

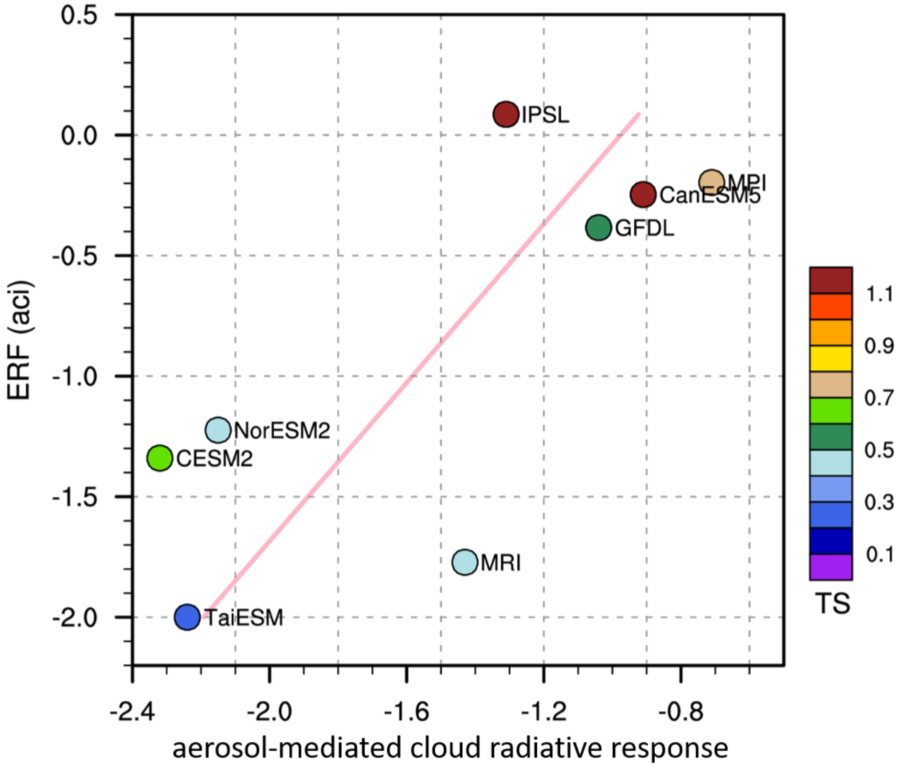

Figure 7. Inter-model comparison of aerosol–cloud diagnostics derived from cloud radiative kernels and APRP decomposition. The x-axis shows the kernel-derived aerosol-mediated cloud radiative response (W m^{-2}), and the y-axis shows the APRP-derived aerosol–cloud interaction forcing, ERFaci (W m^{-2}), for TaiESM1 and selected CMIP6-class models. Marker colors indicate the TS changes between historical and piControl, and the pink line shows the linear least-squares fit across models.

https://doi.org/10.5194/egusphere-2026-4942
Preprint. Discussion started: 19 August 2026

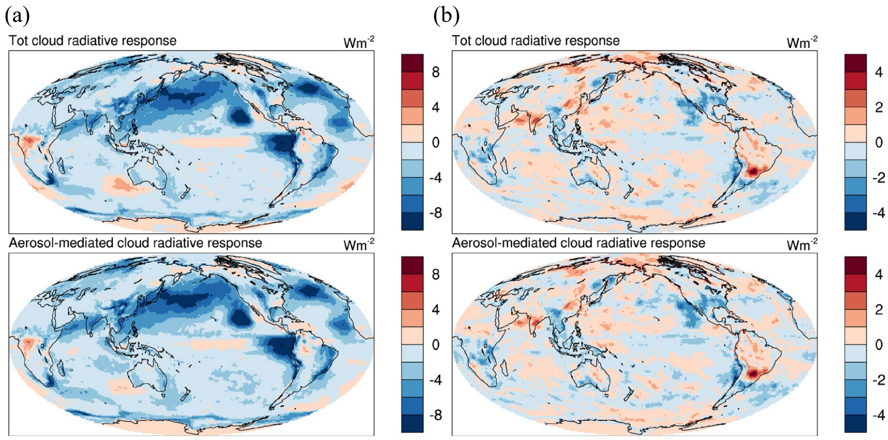

Figure 8. Cloud radiative response associated with (a) prescribed-SST historical forcing (hisSST-piControl) and (b) interactive ocean adjustment (historical-hisSST) in TaiESM1. The top row shows the total cloud radiative response, and the bottom row shows the aerosol-mediated cloud radiative response, both in W m^{-2}.

https://doi.org/10.5194/egusphere-2026-4942
Preprint. Discussion started: 19 August 2026

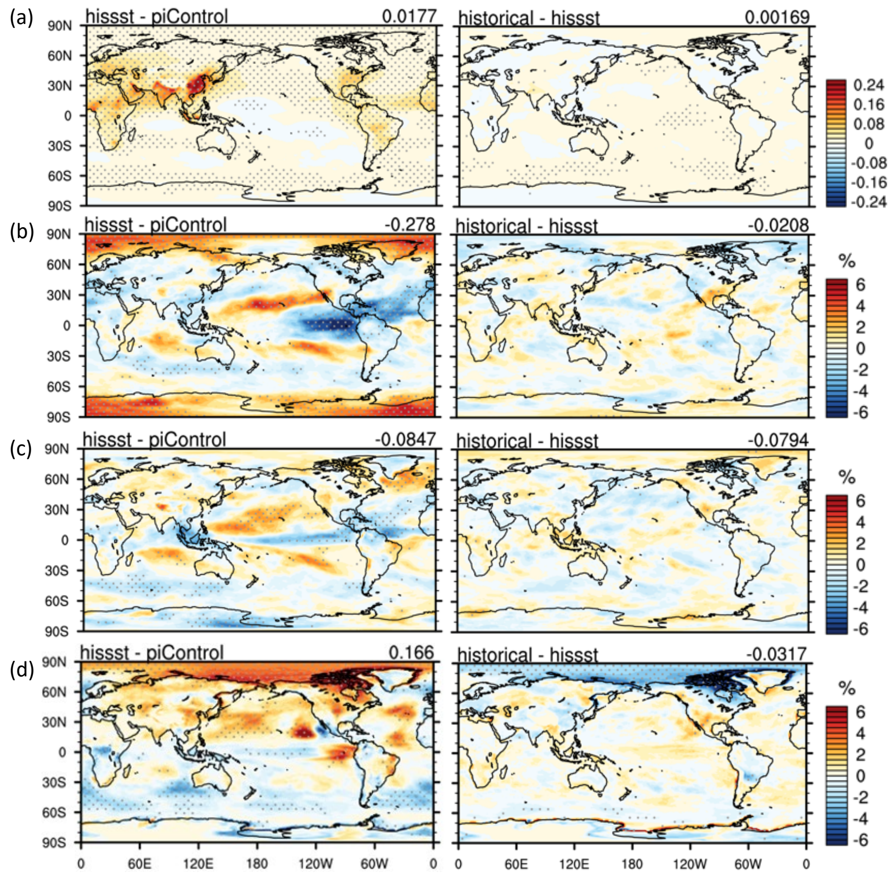

Figure 9. Annual-mean differences in aerosol loading and cloud fraction in TaiESM1. Shown are differences in (a) aerosol optical depth (AOD), (b)high-level cloud fraction, (c) middle-level cloud fraction, and (d) low-level cloud fraction (in %) for the prescribed-SST historical response (histSST – piControl), and the interactive-ocean adjustment (historical – histSST). Numbers in the upper-right corner of each panel indicate global-mean differences.

https://doi.org/10.5194/egusphere-2026-4942
Preprint. Discussion started: 19 August 2026

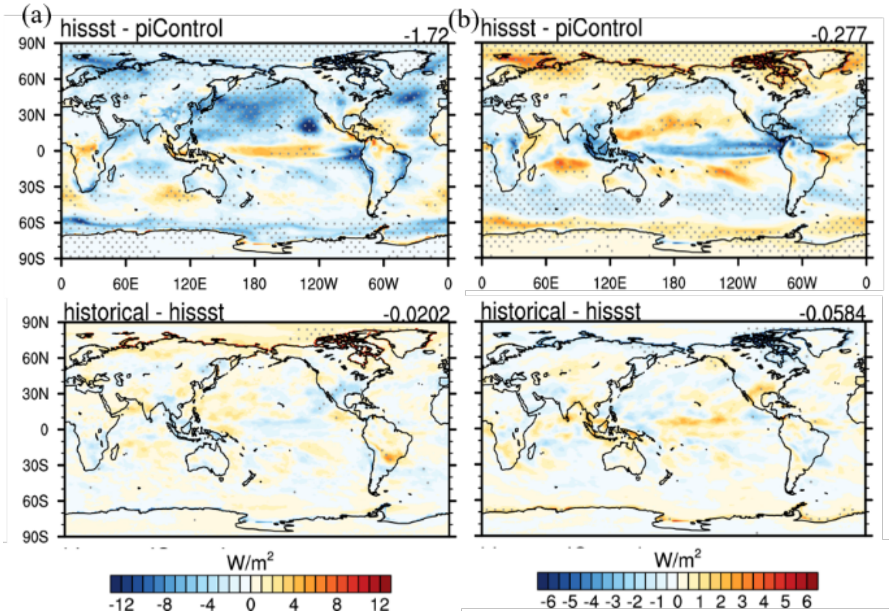

Figure 10. Annual-mean differences in shortwave and longwave cloud radiative effects in TaiESM1. The left column shows the shortwave cloud radiative effect (SWCF; W m^{-2}), and the right column shows the longwave cloud radiative effect (LWCF; W m^{-2}). The top row shows the prescribed-SST historical response (histSST – piControl), and the bottom row shows the interactive-ocean adjustment (historical – histSST). Numbers in the upper-right corner of each panel indicate global-mean differences. Stippling denotes regions where the differences are statistically significant at the 95% confidence level. Note that different color scales are used for SWCF and LWCF.